Dissimilar Friction Stir Lap Welding of AA2198 and AA7075 Sheets: Forces, Microstructure and Mechanical Properties

Antonello Astarita (antonello.astarita@unina.it)
Dept. of Chemical, Materials and Production Engineering, University of Naples “Federico II”, P.le Tecchio 80, 80125, Naples, Italy

Fausto Tucci
Dept. Of Industrial Engineering, University of Salerno, Via Giovanni Paolo II 132, Fisciano, Italy.

Alessia Teresa Silvestri
Dept. of Chemical, Materials and Production Engineering, University of Naples “Federico II”, P.le Tecchio 80, 80125, Naples, Italy

Michele Perrella
Dept. of Chemical, Materials and Production Engineering, University of Naples “Federico II”, P.le Tecchio 80, 80125, Naples, Italy

Luca Boccarusso
Dept. of Chemical, Materials and Production Engineering, University of Naples “Federico II”, P.le Tecchio 80, 80125, Naples, Italy

Pierpaolo Carlone
Dept. Of Industrial Engineering, University of Salerno, Via Giovanni Paolo II 132, Fisciano, Italy.

Research Article

Keywords: FSW, dissimilar joint, lap joint, aluminum alloys, microstructure, force analysis, mechanical properties

Posted Date: March 4th, 2021

DOI: https://doi.org/10.21203/rs.3.rs-252238/v1

Version of Record: A version of this preprint was published at The International Journal of Advanced Manufacturing Technology on August 4th, 2021. See the published version at https://doi.org/10.1007/s00170-021-07816-7.

Abstract

This paper deals with the dissimilar friction stir lap welding of AA2198 and AA7075 sheets. The influence of processing parameters, namely welding speed and tool rotational speed on joint features, microstructure, and mechanical properties were investigated implementing a full factorial design of experiments. During the welding process, axial and transversal forces were continuously measured using a dedicated sensed fixture aiming at the correlation of this processing parameter with the quality of the achieved joints. The reported outcomes showed a very narrow processing window in which it was possible to avoid the formation of defects while the formation of an hook was observed for all the joints welded. The influence of the weld bead morphology on the lap shear strength was elucidated proving that the strength is ruled by the hook morphology. A correlation between the process parameters and the forces arising was also attempted. The final microstructure of the joints was studied and explained and also compared with the microhardness results.

1. Introduction

Aluminum alloys belonging to 2xxx and 7xxx series are increasingly used in the aerospace industry to realize multi-material welded or assembled structures. Clear evidence of the advantageous combination of different materials is represented by fuselage panels of aircraft, that are usually made of AA 2024 skins and strengthened by lap joining of AA 7075 stringers as reported by Dubourg et al. [1] in their paper, where the fabrication of these joints were carefully studied. Friction stir welding (FSW) process is considered to be sufficiently mature to be developed for aircraft manufacture, Astarita et al. demonstrated that if compared to fusion welding FSW leads to the reduction of metallurgical defects and distortion[2]; in a different work Astarita et al. (2012-a) showed also that weight savings of up to 15% and cost savings of 20% can be achieved by its application [3]. Simar and Avettand-Fènoël [4] demonstrated also that FSW can be considered a viable technique to join dissimilar aluminum alloys in distinct configurations. Paulo et al. demonstrated that the presence of an FSW joint affects the overall mechanical behavior of a component, while Sudhagar et al. proved that the process parameters adopted determine both quality and structural properties of the final part [5, 6]. Baraka et al. (2015) found that the material reactions to the tool penetration and advancement are precious information for the online process monitoring and for the dynamic reprogramming of the operative parameters [7]; moreover Mishra et al. stated that these aspects are particularly relevant in the current context of the industry 4.0 by proving their influence on the overall performance of a manufacturing system [8].

In the past decades, a relevant amount of work has been spent to the process for similar and dissimilar welding of Al-Li and Al-Zi-Mg alloys, Alam and Sinha published an interesting review paper reporting the most of the attempts made in literature to weld the third series Al-Li alloys while Paradiso et al. investigated the dissimilar welding of Al-Li alloys with magnesium alloys proving the feasibility of the process in a very marrow processing window [9, 10]. Williams and Starke [11] stated that these Al-Li alloys can be considered optimal candidates for aerospace and aircraft vehicles, due to low density, high specific modulus and specific strength, the same consideration has been drawn by Goebel et al. a latest

study considering the latest developments of Al-Li alloys. Yin et al. [12] reported that the alloys belonging to the recently developed third generation of damage-tolerant Al-Li alloys, such as AA2198, demonstrated relatively higher mechanical properties, Zhang S. et al. [13] stated that these high mechanical properties can be attributable mostly to the precipitation of the T_1 (Al_2CuLi) phase, whereas Milagre et al. [14] proved that the attendance of Li lower density and enhance stiffness. In contrast Xu et al. [15] and lately Krug et al. [16] reported that the previous generations of Al–Li alloys, e.g. 2020 alloy (Al–1.21Li–4.45Cu–0.51Mn–0.20Cd, in wt%) and 8090 alloy (Al–2.5Li–1.11Cu– 1.16Mg–0.16Zr, in wt%) exhibited limited ductility and significant anisotropy in mechanical properties.

Recent papers demonstrated the feasibility of similar FSW of AA2198, even if they were focused on the butt joint configuration. Among others, Ma et al. [17] highlighted a very narrow processing window and a remarkable influence played by processing parameters on both fatigue life and tensile strength. Buffa et al. [18] demonstrated the weldability of AA 2098 through friction stir welding and pointed out a big influence of the processing conditions on the mechanical properties of the joints. Cavaliere et al. [19] proved that the strength of the joint is also influenced by the relationship between rolling and welding direction. In a subsequent work Cavaliere et al. [20] better elucidated the reasons of this anisotropy. Gao et al. [21] studied the strengthening mechanism, the microstructure and precipitation evolution in the different metallurgical zones of the joint and provided a comprehensive overview of the phenomena occurring across the joint, once again they used butt joints welded by using optimized process parameters available in literature. Tao et al. [22] elucidated the crack propagation and the failure modes of AA 2198 friction stir welded butt joints, they claimed that the transition zone between the stirred zone and the thermomechanical affected zone is the weakest part of the joint.

Gibson et al. [23] published one of the first studies reporting the similar friction stir lap welding of AA 2198 sheets and testing their mechanical behavior. The joints produced at welding speeds of 200 and 350 mm/min exhibited higher ultimate load in tension-shear testing, compared to joints welded at 75 mm/min. Moreover, the blanks welded using tool rotational speeds of 1200 rpm and 1500 rpm resulted remarkably more resistant than the ones welded at 900 rpm. Reimann et al. [24] recently proposed a study where an attempt to AA2198 FSW process monitoring by force analysis was reported. They demonstrated the influence of forces on heat input, but the relationship with the processing parameters was not exhaustively investigated. The lack of consolidated knowledge in friction stir lap welding of AA2198 alloy is even more evident when dissimilar joints, based on the combination of 2xxx and 7xxx series, are considered. In general, FSW of 2xxx and 7xxx series has been studied in the last years, but most studies were devoted to well-known alloys, such as AA2024. Song et al. [25] provided a comprehensive study on the overlap welding between AA 2024 and AA 7075. Venkateswaran and Reynolds [26] investigated the influence of the processing parameters and of the weld bead morphology on the mechanical properties of AA2024/7075 lap joints produced by FSW. They commented that there are two main factors affecting the tensile strength of FS welded lap joints: effective sheet thickness (EST) and the sheet interface shape (hooking). Dubourg et al. [1] reported that the material hooking was a determinant for the mechanical properties of the joint, they particularly studied the overlap FSW of AA

2024 and AA 7075. Jandaghi et al. [27] studied the dissimilar friction stir welding between AA 2198 and AA 7475 in butt joint configurations, they investigated the complex metallurgical evolutions and also studied the influence of post welding heat treatments. Literature concerning FSW of AA2198 with 7xxx series alloys is very scarce.

Looking at the available reports, it seems that a comprehensive understanding of AA2198 and AA7075 FSW in overlap configuration, even if desirable considering the opportunities in the aerospace sector, is yet to be reached. Similarly, dedicated studies providing a better understanding of force arising during the friction stir welding of AA 2198, even in butt joint configuration, are not exhaustive to the scope of process monitoring. The present paper is focused on the dissimilar FSW of AA 2198 to AA 7075 in the lap joint configuration with the aim to provide a contribution to fill the indicated gap of knowledge. Different processing conditions were explored by varying the main process parameters, assuming a full factorial design of experiments based on three values for the tool rotational speed and two values for the welding speed. During the process, selected force components have been acquired using a dedicated fixture equipped with a load cell. Finally, a detailed microstructure and mechanical characterization were performed by optical and SEM analysis, lap shear testing and microhardness measurements, attempting to correlate the joint quality with in-process collected data. Under the light of the reported outcomes, the following open questions have been addressed: i) which is the suitable processing window for the considered welding configuration; ii) which is the trend of the forces during the process and how processing parameters influences the force profile; iii) which is the microstructure induced by the action of the tool in correlation with the variation of processing parameters; iv) how processing parameters and microstructural aspects influences the mechanical properties of the joint.

2. Materials And Methods

In the present investigation, AA2198 T351 (200x100x3.2 mm^3) Al alloy and AA7075 T6 (200x100x2 mm^3) alloy sheets were used as base materials. Astarita et al. and Velotti et al. reported the nominal compositions and the mechanical properties of these alloys which are not reported here in the interest of brevity [28, 29]. A CNC machine (FAMUP MCX 600) operating in displacement control mode was employed. Welding processes were conducted positioning the AA2198 on top and AA7075 on the bottom of the overlap configuration, adopting an overlap length of 25 mm. The adjoining surfaces of both plates were cleaned with a stainless-steel brush and acetone before the welding process. An additional sheet was placed under the AA2198 plate to avoid undesired displacement. This setup was finally clamped on the backing plate and fixed on a Kistler™ three-axis dynamic dynamometer positioned on the machine table, to detect force components. More specifically, the in-plane welding force (hereinafter F_x) acting parallel to the welding direction and the downward forging (hereinafter F_z) perpendicular to the plane of the sheet, generated during the process, were continuously measured. A schematic and some pictures of the welding setup are showed in Fig. 1.

An H13 steel tool, characterized by concave shoulder and tapered left-hand threaded pin, was used in this work. The tool was kindly supplied by FPT Industrie SPA. Tool dimensions are reported in Fig. 1. The

selection of tool geometry was based on the following considerations: i) tapered threaded pin introduces a vertical component in the stirring action enhancing material flow and ii) pin length major than the thickness of the top plate allows the pin to be plunged inside the bottom sheet providing a weld interface based on mechanical locking; alternatively, materials joining relies only on the formation of a relatively weaker conversion layer at the interface. Venkateswaran and Reynolds [26] studied the factors affecting friction stir welding of dissimilar aluminum alloys and they also suggested that a pin length major than the thickness of the top plate allows the pin to be plunged inside the bottom sheet providing an higher strength for the joint.

The details of the experimental campaign are given in Table 1. The design of experiment (DOE) is based on the variation of the main process parameters, in terms of tool rotational speed (TRS) and welding speed (WS). In the same table, the revolutionary pitch, defined as the ratio between TRS and WS, is provided. In each case, the tool was rotated clockwise and tilted 2° forward to improve the tool shoulder forging action, the shoulder was plunged for 0.2 mm in the top sheet.

Table 1
Experimental campaign carried out, indication of all the samples welded.

Tool Rotational Speed [rpm]	Welding Speed [mm/min]	Revolutionary Pitch [rot/mm]
1200	60	20
1500		25
1800		30
1200	120	10
1500		12,5
1800		15

After the joining process, the morphology of the welded crown of each sample was observed and measured, with respect to the relevant dimensions, by means of confocal microscopy (LEICA DCM 3D). From each weld, three metallurgical specimens were extracted for macroscopic, microscopic, and microhardness characterization of the cross section orthogonal to the weld line of each joint. For the metallurgical observations and analysis, the extracted pieces were mounted by using a conductive thermoplastic resin supplied by Struers (Lucite) and, after that, ground with SiC papers and then lapped using diamond suspension down to 1 μm to achieve a mirror-like finishing. Samples were etched by using Keller etchant for 15 s to unveil the significant metallurgical features. A metallurgical microscope (Olympus GX71) equipped with an Olympus digital camera (XC50) and a scanning electron microscope (Hitachi TM3000) equipped with a National Instruments EDX microprobe (Oxford Instrument Swift ED3000) were used to observe the microstructure of the welding zones, and to detect eventual IMCs precipitation. Vickers micro-hardness tests were carried out under an indentation load of 100 g for a dwell

time of 15 s by using a Leica QVMHT Hardness Tester. The distance between indentations was equal to 0.5 mm. The mechanical properties of the joints were assessed by lap shear testing, according to the ASTM D1002 standard (Standard Test Method for Apparent Shear Strength of Single-Lap-Joint Adhesively Bonded Metal Specimens by Tension Loading, Metal-to-Metal) and using an MTS Insight universal testing machine. Five specimens, 25.4 mm in width, were cut from each joint. The grip area was defined as 25.4 mm^2, whereas opportune tabs were used to avoid undesired stress components. As already illustrated by Perrella et al. [30], for the preparation to the test, the sides of the specimens were polished and then painted by using acrylic varnish to obtain a speckle pattern. During the lap shear test, an industrial uEye camera equipped with a 25mm objective was used to record the failure mode of each sample.

3. Results And Discussion

3.1. Forces Analysis

A qualitatively similar trend was detected for the force components F_x and F_z for all the performed welding processes. A representative plot, related to the 1200/60 welding conditions, is shown in Fig. 2.

As intuitive, force components are influenced by the material flow in the region surrounding the tool pin, Boccarusso et al. [31] proved that the force profiles are strictly dependent on the specific processing stage, namely plunging, dwelling and welding (or travelling) phases. These stages are described below and are called phase I, phase II and phase III:

i. Phase I corresponds to the tool plunging. it starts when the rotating pin approaches the upper surface of the AA2198 sheet (generating a first F_z peak, indicated as A in Fig. 2), and bring to an end when the top sheet is fully crossed by the pin and the desired plunging depth has been reached. A second F_z peak (indicated as B) has been detected when the shoulder was approaching the top surface and the pin was plunged inside the AA7075 sheet. This second peak results higher than the former one due to the larger contact area between the shoulder and AA2198 surface and the higher resistance of the 7075 sheet at relatively lower temperature Noticeably, in phase I, the Fx is close to zero. The plunging velocity was defined as equal to the welding speed for each condition.
ii. Phase II includes a dwelling time of 15 s. A localized rise of the temperature is caused by the rotational movement of the pin in the unmodified position. Phenomenon ascribed to the generated frictional heat. The induced material thermal softening implies a reduction in the resistance to tool plunging. Consequently, F_z decreases approaching a local minimum at the end of phase II.
iii. During phase III, which represents the concrete welding, the tool proceeds along the joint line, promoting a continuous mixing and bringing together the materials. It is visible that, initially, component F_z exhibits a further local peak, indicated as C, before stabilizing on a reasonably steady state value. As expected, at the beginning of this phase, the component F_x sharply raises caused by the movement of the tool along the x-direction and inherent resistance to material displacement.

Figure 3 summarizes the values of the A and B peaks (related to the F_z force component) as well as the steady state values of both components, for all the welded joints. As reasonably expected, the value of the vertical force, F_z, is always considerably major than the in-plane one, F_x.

Collected data clearly pointed out the influence of the processing parameters on the peak values A and B exhibited by the component F_z during the plunging phases. As a matter of fact, increasing the rotational speed involves that a higher quantity of frictional heat is released at the material-tool interface,, causing a more significant material softening. Therefore, smaller downward vertical forces are needed to plunge the tool at the planned depth. Zimmer et al. [32] also observed that the forces are influenced by the processing parametrs and in particular that a lower downward vertical force is required when the heat input is increased. The two peaks, A and B, are roughly of the same magnitude because the mechanical properties of the two aluminum alloys are substantially similar. Boccarusso et al. [31] studied the friction stir lap welding of AA6082 aluminum alloy to AZ31 magnesium alloy and found a different evidence, i.e. a noticeably difference between the two peaks, that can be attributable to the distinct mechanical properties of the investigated materials. Conversely, lower values for F_z force were detected during the plunging stage lowering the welding speed, since the plunging speed was accordingly reduced. In fact, assuming the rotational speed as a constant, the same amount of heat is generated and dissipated into the material. Obviously, if the penetration of the tool inside the sheets is relatively slower, more time is left to heat diffusion across the thickness, and this leads to a more pronounced softening of the material. Steady state values of both F_z and F_x components are plotted in Fig. 3 (c and d) as a function of the processing parameters. Astarita et al. [33] assert that, referring to the friction stir butt welding, both F_z and F_x components present a monotonic growing when increasing the Welding Speed for a fixed Tool Rotational Speed and, on the other hand, present a monotonic decrease when increasing the TRS for a given WS. Indeed, the softening phenomena are strongly related to the material resistance and flow conditions, whereby the major the heat input is, the minor the force is itself. Similar considerations can be drawn considering force components variation as a function of the revolutionary pitch. In fact, higher revolutionary pitch involves a higher heat input leading to a more significant material softening and lowering of the forces.

3.2. Macroscopic and microstructural observations

Representative images of the top surface of the joints, including a macroscopic view of the cross sections are reported in Fig. 4. It can be immediately observed that for all the considered combinations of processing parameters, material continuity at the interface between the top and bottom sheets was successfully achieved. Nevertheless, for processing conditions except 1500/60 and 1200/60, internal defects, namely grooves and tunnels following the nomenclature proposed by Mishra and Ma [34], were detected (highlighted by white arrows in Fig. 4). It can be deduced that defect formation in the cross section can be avoided only working within a narrow range of revolutionary pitch (roughly from 20 to 25).

Figure 5 represents the microhardness distribution on the welding cross-section. The microhardness contours are reported over the optical microscopy acquisitions of the samples cross-section, after the

lapping, polishing and chemical etching.

From a qualitative point of view, each joint, except the one welded at 1200/120, showed a similar microstructure, characterized by a clearly visible nugget zone (NZ) exhibiting the typical onion ring structure. Also, an evident formation of lateral hooks of AA7075 penetrating within the AA2198 top layer and encapsulating the nugget area is appreciable. The slight plunging of the tool into the bottom sheet, necessary to generate a bonding region, promotes the upward extrusion of the material from the interface toward the stirred zone (SZ). Song et al. [25] highlighted that this vertical flow of material is responsible for the formation of the hook-shaped macrostructure.

A slightly different appearance is showed by the joint welded at 1200/120, representing the processing conditions characterized by the lowest heat input. The onion ring structure is still clearly visible, but, differently from other samples, there is only one short hook in the advancing side. This outcome suggests that the formation of the hooks is ruled by the amount of heat generated during the process and the heat transfer within the material, Carlone and Palazzo [35] demonstrated that the formation of these hooks is facilitated at higher heat input and material softening. In concept, hook formation can be considered as a jetting phenomenon, ruled by the plunging pressure and the viscosity of the softened material.

The microhardness maps reflect the material flow described in the previous sections. An increase in microhardness was detected in the region of each hook. This evidence is consistent with the SEM observations that showed that the hooks are made of recrystallized grains that experienced a severe work hardening. It is also possible to appreciate that the global hardness of the joint increases with the decrease of the TRS, i.e. increase with the decreasing of the heat input. Mehta et al. [36] in their study on the conventional and cooled friction stir welding also observed that the global hardness of the joints increases with the decrease of the TRS.

In what follows, high magnification micrographs, captured with both optical microscope and scanning electron microscope, are provided to highlight the microstructures established by the process.

Figure 6 provides some details of the metallurgical features detected in the observed cross section. In particular, the joint welded at 1500/120 was here used as representative one in the interest of brevity.

Recalling the standard terminology used in friction stir welded joints, the nugget zone (NZ) is defined as the region of the weld bead which experienced a full recrystallization due to the action of the tool. Astarita et al. stated that the thermomechanical affected zone (TMAZ) is the region of the weld bead, adjacent to NZ, where the grains appear highly deformed but not fully recrystallized [3]. By adopting this classification, a very interesting NZ can be identified. Fully recrystallized zones can be observed in the center of the joint, where the onion ring structure made of AA 2198 is well evident (see Fig. 6e and Fig. 6d), at the boundary between AA2198 and AA7075 (Fig. 6f); in the hook region in the retreating side (see Fig. 6a and Fig. 6h); and, finally, in the flow arm region (see Fig. 6c). From this observation, it can be claimed that the NZ is made of four different subzones: the onion ring region (made of AA 2198), the flow arm region (made of AA 2198), the inner part of the hooks, i.e. the side of the hooks adjacent to the onion

rings, (made of 7075), the upper part of the 7075 sheet. In Fig. 6b, the very thin tip of the hook, surrounded by fully recrystallized AA2198 grains, is visible, supporting the evidence that the hook penetrated in the AA2198 nugget zone. On the other hand, Fig. 6h points out that the root of the hook is in between the fully recrystallized grains of the NZ and the stretched grains of the TMAZ. Interestingly, the hook itself seems to be made of two different regions, which experienced, respectively, a full recrystallization or a grain stretching. Concerning the TMAZ two different areas have been observed, constituted, respectively deformed grains of AA2198 (Fig. 6a) and of AA7075 (Fig. 6g-h). Carlone et al. proved that the heat affected zone (HAZ) cannot be easily identified at these magnifications since it is only characterized by a different distribution of the second phase back particles [37]. This peculiarity has been generally observed for several aluminum alloys.

The presence and morphology of the hooks significantly influence the mechanical strength of friction stir welding lap joints; nevertheless, there is no agreement about the actual role played by this feature. Naik et al. pointed out that the hook represents an interpenetrating feature creating a mechanical interlocking conditions that enhances the tensile strength of the joint [38]. On the other hand, Chowdury et al. reported that hooks materialize preferential paths for crack propagation, negatively affecting the resistance of the joint [39]. Detailed high magnification micrographs for the hook in the advancing side and in the retreating side have been reported in Fig. 7 and Fig. 8. From those figures, it is immediate to observe that both hooks are made of fully recrystallized equiaxial and very fine grains. Furthermore, hooks are clearly distinguished from the onion rings region, which is made of AA2198, suggesting that the hook formation is related to the upstream material flow of AA7075 from the bottom sheet.

The present study also highlighted the formation of a crack in the advancing side between the hook and the AA2098 TMAZ (see Fig. 7) while complete material continuity was detected between the aforementioned hook and the nugget zone (Fig. 8). This occurrence can be explained taking into account the material flow leading to the hook formation and considering that, with reasonable approximation, i.e. neglecting the tilt angle (2°), the tool axis is perpendicular to the faying surfaces of both sheets. This geometrical condition prevents an effective breaking action of the oxide layers at the sheet interface, differently from what is typically observed in friction stir butt welding. Consequently, complete material continuity is prevented due to the presence of the oxide layer. The hook formed in the retreating side showed a similar evidence, but the crack is extremely narrow and is not continuous if compared to the previous case, suggesting the creation of a weak region in the advancing side of the joint. To summarize, it is possible to claim that hooks exhibit a crack-like unbonded interface generated by the tool during the stirring from the original faying surfaces on both the advancing and retreating sides. The difference between the transition from the hook to the surrounding region in the advancing and retreating side has been related to the material flow pattern promoted by the stirring action of the tool. In fact, the material is continuously transferred from the advancing to the retreating side, inducing a compression and crack closure effect in the retreating side and generating a lack of material in the advancing side.

The hook morphology is closely related to the material flow and deformation as well, consequently, some differences are detected comparing the hook shape and size in the advancing and retreating sides.

Figure 9 reports the height of the hook, in both advancing and retreating sides, as a function of processing parameters. Indeed, the plastic flow of the material is asymmetric on the two sides, being rotational and welding speed concordant in the AS, where a higher hook is formed, but opposite on RS, exhibiting a slighter smaller hook. What is more, being flow velocities influenced by the processing parameters, an obvious influence on hook height is expected. The influence of process parameters on the hook height was not definitely clarified. In fact, the joint welded using the lower heat input (1200/120, corresponding to a revolutionary pitch of 10) showed the lowest values of the hook height (the retreating side hook was almost absent). Then a sharp increase in the hook height was fount for revolutionary pitch equal to 12.5 (1500/120), followed by a decrescent trend. Consequently, a clear correlation between hook height and heat input was not found. From the analysis of the cross sections, reported in Fig. 5 it can be claimed that also the width of the hook is influenced by the process parameters. As an interesting outcome, the maximum measured hook height is associated to the joints welded adopting 1500 rpm as TRS; apparently a further increase of the TRS (with a consequent rise in the heat input and a more pronounced softening of the material) leads to the formation of a thicker but shorter hook.

The bottom sheet plunging, defined as the maximum depth reached by the NZ underneath the interface between the two sheets to be welded, was found to increase with the increase of the heat input. Babu et al. [40] also showed that an higher heat input implies the widening of the recrystallized NZ toward the bottom sheet.

Aiming to better understand the metallurgical evolutions occurring during the process, the microstructures in the different zones of the welding are given in Fig. 6.

The SEM micrographs of the base materials (BM) in both the alloys (Fig. 10a and Fig. 10d) show a pancake microstructure typical of rolled products, the grains are flattened and stretched along the rolling direction. Some precipitates, easily attributable to the heat treatment used for the BM, are also evident, in particular for the AA7075 alloy, coherently with the different strengthening mechanism.

Figure 10b and Fig. 10e show micrographs of the TMAZ of both AA2198 and AA7075, as detected by SEM observations in the spots indicated in Fig. 6a and Fig. 6h. Stretched, highly deformed and partially recrystallized grains are clearly visible. Furthermore, the grain size appears to be similar for the two alloys. As evident, grains were stretched following the material flow, so along the mixing pattern imposed to the material by the stirring action of the tool.

In Fig. 10c and Fig. 10f, SEM micrographs taken in the fully recrystallized zone are reported. Both AA2198 and AA7075 grains are equiaxed and refined with respect to the BM structure, Astarita et al. in their work also found that the fully recrystallized grains are smaller than the ones of the base material [41]. It is also possible to see that the 7075 grains are smaller than the 2198 ones. This evidence can be explained recalling the recrystallization laws, enunciated by Cahn and Haasen [42]ga, stating that the final grain size is ruled by: i) the initial grain size, ii) the amount of plastic deformation experienced by the material, iii) the local temperature experienced during the deformation, iv) the duration of the exposure at recrystallization temperature or above, v) the properties of the material. Furthermore, it should be

considered that the higher the strain rate, the lower the recrystallization temperature, therefore, for a given temperature cycle, higher strain rate implies a more prolonged exposure to temperature exceeding the recrystallization condition. In the investigated case, the two alloys exhibited a very similar initial grain size; nevertheless, the material of the bottom sheet (AA7075) experienced lower temperatures and a lower amount of plastic deformation during the welding process. Zhou et al. [43] discussed that during hot forming processes, such as friction stir welding, aluminum alloy is liable to undergo dynamic recrystallization (DRX), which affects the crystallographic texture and thus mechanical properties. Kim and Yoo [44] demonstrated that the occurrence of DRX leads to the formation of refined equiaxed grains. Dehghan-Manshadi et al. [45] proposed a general descriptive model for DRX where it was stated that the nucleation of DRX grains can start at a critical strain which is a function of initial microstructure and deformation conditions (i.e. temperature and strain rate). Then, the evolution of DRX microstructure can proceed further by increasing deformation and through the formation of an equiaxed, refined microstructure. Ueki et al. proved that both temperature and strain rate, as well as the amount of plastic deformation, have a pronounced influence on the final DRX structure [46]. What is more, for a metal material, a pronounced interaction between microstructure evolution and mechanical property exists during a plastic forming process, so the occurrence of DRX and its understanding is fundamental to better understand the whole process. To date there are no detailed papers describing the DRX behaviour of 2198 alloy during plastic deformation. Some considerations can be drawn following the work conducted on AA2024. Zhang X. et al. [47] studied the axial compression of AA2024 billets by varying temperature and strain rate. They demonstrated that the temperature governs the atomic diffusion and the driving force of dislocation migration while the strain rate controls the dislocation density and the accumulation energy of the grain boundary; they observed that the recrystallization temperature ranges from 523 and 723 Kelvin depending on the strain rate and the initial microstructure. Quan et al. [48] carefully studied the general recrystallization mechanism and the influence of strain, strain rate and temperature on DRX behaviour of as-extruded 7075 aluminum. They also proved that the recrystallization temperature is depending on strain rate and initial microstructure, a reasonable range for this temperature was 573–723 Kelvin.

As far as the materials involved in this investigation are regarded, it should be considered that the dynamic recrystallization temperature of AA7075 is slightly higher than AA2198, and that the latter one was further reduced by the relatively higher strain rate, explaining the more refined grain structure induced by the welding process in the AA7075 sheet.

3.3. Lap shear test

In this paragraph, the results provided by lap shear testing are discussed. Load-displacement curves, measured for all joints, are reported in Fig. 11.

Satisfactory repeatability was found for all the processing conditions. Two branches can represent the trend of load-displacement curves. The former is quite linear, with a slope representing the initial linear stiffness of the joint. The latter, at first almost linear even if with a different slope from the first branch,

shows the effects of plate element plasticization and bending occurrence due to progressive specimen fracture. This tensile behavior is more evident in the specimens presenting higher hooks.

All the specimens presented a progressive increase of load up to final sudden failure, except some that highlighted a saw tooth load-displacement pattern. In this case, the failure mechanism of FSW joints was associated to the separation of plate elements along the interface surface. Interestingly, the highest tensile properties were exhibited by the joint 1200/120, independently of the internal tunnel, see Fig. 4. It should be noted that for this joint an evident hook in the advancing side was not detected, supporting the thesis of the detrimental effect played by the hook on the mechanical behavior of the joint. Furthermore, it is worth noting that the influence of the hook is dominant with respect to the other internal defects.

A representative failed sample per each set of welding parameters is shown in Fig. 11. Two distinct failure modes were observed. Mode A corresponds to tensile fracture starting from the crack at the tip of the hook on AS, propagating upwards along the cracked interface between the hook and the TMAZ and finally fracturing the SZ at the interface between the onion ring zone and the flow arm. This fracture mode was exhibited by all the joints, being the joint 1200/120 the only exception. This joint showed a shear fracture mode (B), where the failure occurs along the original lap interfaces of the two sheets. It is worth noting that the 1200/120 joint is the one exhibiting a negligible hook formation. The joint that failed with the mode B showed the highest ultimate load, further supporting the hypothesis of the detrimental role of the hook with respect to the mechanical properties.

Fersini and Pirondi [49] stated that the effect of hook on the lap joint strength can be quantitatively analyzed introducing the effective sheet thickness (EST). In the present investigation, the EST on the advancing side was considered. The EST is defined as the minimum sheet thickness from the tip of the hook to the top surface of the upper sheet, while the lap shear strength has been calculated as the ratio between the measured failure load and the equivalent section (defined as the product between the measured EST and the width of the tensile specimen). The results are plotted, against processing parameters, in Fig. 12.

The higher lap shear strength was shown by the joints welded adopting a TRS value of 1500 rpm, while the higher failure load was shown by the 1200/120 joint. This occurrence has been explained considering that joints welded at 1500 rpm were free from internal defects, independently of the welding speed, while 1200/120 joints showed an internal tunnel. Interestingly, while the load at failure provides information regarding the strength of the joint, the shear strength (calculated as previously defined) provides information about the eventual presence of internal defects.

Generally, the mechanical properties are expected to decrease with the increase of the TRS and decrease with the decrease of the WS. From Fig. 12, it is possible to observe that the strength decreases with the increasing of the heat input, Cavaliere et al. [50] also found that the best mechanical properties are achieved with the lowest values of the heat input, claiming “coldest is the better”. In the investigated case, a more significant influence of the TRS on the mechanical strength was found.

4. Conclusions

Taking into account what herein reported and discussed, the following conclusions can be drawn, attempting to provide some answers to the questions formulated in the introduction of the manuscript:

- The feasibility of the dissimilar joining by friction stir welding of AA 2198 to AA 7075 in lap joint configuration has been demonstrated for different processing conditions. Internal and superficial defects (mainly grooves and tunnels) were found for all of the welding produced using advancing speed of 120 mm/min and for the samples processed adopting tool rotational speed of 1800 rpm; but a processing window leading to sound joints has been framed and clearly defined.
- Force trend varies during the plunging, dwelling and travel phase, exhibiting several peaks. Forces increase when decreasing the heat input, i.e. when increasing with the increase of the welding speed and with the decrease of the tool rotational speed. The recorded values of the Fz were always higher than the ones recorded for the Fx.
- An onion rings structure, made of recrystallized grains, was clearly visible in the nugget zone. The nugget zone was constituted by very thin and fully recrystallized equiaxial grains, whereas a more significant refinement was found for the grains of AA7075. Grain refinement was detected also in the flow arm. Hooks were formed in both the advancing and retreating sides, due to the upward flow of AA7075 from the bottom plate. Thermomechanical affected zones, made of highly deformed and partially recrystallized grains, were also identified.
- Lap shear tests highlighted that the presence and size of the hook, rather than internal defects, are the main factor ruling the failure load. The achieved result supports the hypothesis, already claimed in literature, that the hook has a detrimental influence on the strength of the joints, creating de facto as a preferential path for the crack propagation.
- The microhardness map reflected the different metallurgical zones observed, whereas higher microhardness values where measured in correspondence of the highly deformed and recrystallized grains of the hooks. The microhardness values measured in the nugget zone were slightly higher than the ones of the BM, whereas lower values where associated with the heat affected zone. As a general trend, the hardness increases with the decreasing of the heat input, consistently with what typically happens in FSW.

Declarations

Funding

This research did not receive any specific grant from funding agencies in the public, commercial, or not-for-profit sectors.

Acknowledgement

Authors gratefully acknowledge Eng. Ilaria Coppola for her support and dedication shown during the experimental activities and also for her enthusiasm that enlightened the days spent in the lab. The authors want also to thank the laboratory LABCAMP^2 (CESMA – University of Naples Federico II) for hosting some of the research activities.

Declarations

Funding (information that explains whether and by whom the research was supported)

The authors received no funding to carry out these activities, they used facilities and raw materials already available in their labs.

Conflicts of interest/Competing interests (include appropriate disclosures)

The authors declare that they have no known competing financial interests or personal relationships that could have appeared to influence the work reported in this paper. The authors also declare that they do not have any conflict of interests.

Availability of data and material (data transparency)

The authors declare that, if required, they will share all the data.

Code availability (software application or custom code)

Not applicable

Authors' contributions

Not applicable

References

[1] L. Dubourg, A. Merati, M. Jahazi, Process optimisation and mechanical properties of friction stir lap welds of 7075-T6 stringers on 2024-T3 skin, Mater. Des. 31 (2010) 3324–3330. https://doi.org/10.1016/j.matdes.2010.02.002.

[2] A. Astarita, U. Prisco, A. Squillace, C. Velotti, A. Tronci, Mechanical characterization by DOE analysis of AA6156-T4 friction stir welded joints in as-welded and post-weld aged condition, Mater. Test. 57 (2015). https://doi.org/10.3139/120.110698.

[3] A. Astarita, A. Squillace, E. Armentani, S. Ciliberto, Friction stir welding of AA 2198 T3 rolled sheets in butt configuration, Metall. Ital. 104 (2012).

[4] A. Simar, M.N. Avettand-Fènoël, State of the art about dissimilar metal friction stir welding, Sci. Technol. Weld. Join. 22 (2017) 389–403. https://doi.org/10.1080/13621718.2016.1251712.

[5] R.M.F. Paulo, F. Rubino, R.A.F. Valente, F. Teixeira-Dias, P. Carlone, Modelling of friction stir welding and its influence on the structural behaviour of aluminium stiffened panels, Thin-Walled Struct. 157 (2020) 107128. https://doi.org/10.1016/j.tws.2020.107128.

[6] S. Sudhagar, M. Sakthivel, P. Ganeshkumar, Monitoring of friction stir welding based on vision system coupled with Machine learning algorithm, Meas. J. Int. Meas. Confed. 144 (2019) 135–143. https://doi.org/10.1016/j.measurement.2019.05.018.

[7] A. Baraka, G. Panoutsos, S. Cater, A real-time quality monitoring framework for steel friction stir welding using computational intelligence, J. Manuf. Process. 20 (2015) 137–148. https://doi.org/10.1016/j.jmapro.2015.09.001.

[8] D. Mishra, R.B. Roy, S. Dutta, S.K. Pal, D. Chakravarty, A review on sensor based monitoring and control of friction stir welding process and a roadmap to Industry 4.0, J. Manuf. Process. 36 (2018) 373–397. https://doi.org/10.1016/j.jmapro.2018.10.016.

[9] M.P. Alam, A.N. Sinha, Fabrication of third generation Al–Li alloy by friction stir welding: a review, Sadhana - Acad. Proc. Eng. Sci. 44 (2019) 1–13. https://doi.org/10.1007/s12046-019-1139-4.

[10] V. Paradiso, F. Rubino, P. Carlone, G.S. Palazzo, Magnesium and Aluminium alloys Dissimilar Joining by Friction Stir Welding, Procedia Eng. 183 (2017) 239–244. https://doi.org/10.1016/j.proeng.2017.04.028.

[11] J.C. Williams, E.A. Starke, Progress in structural materials for aerospace systems , 51 (2003) 5775–5799. https://doi.org/10.1016/j.actamat.2003.08.023.

[12] H. Yin, H. Li, X. Su, D. Huang, Materials Science & Engineering A Processing maps and microstructural evolution of isothermal compressed Al – Cu – Li alloy, Mater. Sci. Eng. A. 586 (2013) 115–122. https://doi.org/10.1016/j.msea.2013.07.084.

[13] S. Zhang, W. Zeng, W. Yang, C. Shi, H. Wang, Ageing response of a Al – Cu – Li 2198 alloy, Mater. Des. 63 (2014) 368–374. https://doi.org/10.1016/j.matdes.2014.04.063.

[14] M.X. Milagre, U. Donatus, C.S.C. Machado, J.V.S. Araujo, R.M.P. da Silva, B.V.G. de Viveiros, A. Astarita, I. Costa, Comparison of the corrosion resistance of an Al–Cu alloy and an Al–Cu–Li alloy, Corros. Eng. Sci. Technol. 54 (2019) 402–412. https://doi.org/10.1080/1478422X.2019.1605472.

[15] Y.B. Xu, W.L. Zhong, Y.J. Chen, L.T. Shen, Q. Liu, Y.L. Bai, M.A. Meyers, Shear localization and recrystallization in dynamic deformation of 8090 Al – Li alloy, 299 (2001) 287–295.

[16] M.E. Krug, D.N. Seidman, D.C. Dunand, Creep properties and precipitate evolution in Al – Li alloys microalloyed with Sc and Yb, Mater. Sci. Eng. A. 550 (2012) 300–311. https://doi.org/10.1016/j.msea.2012.04.075.

[17] Y.E. Ma, Z.C. Xia, R.R. Jiang, W. Li, Effect of welding parameters on mechanical and fatigue properties of friction stir welded 2198 T8 aluminum – lithium alloy joints, 114 (2013) 1–11. https://doi.org/10.1016/j.engfracmech.2013.10.010.

[18] G. Buffa, G. Campanile, L. Fratini, A. Prisco, Friction stir welding of lap joints : Influence of process parameters on the metallurgical and mechanical properties, 519 (2009) 19–26. https://doi.org/10.1016/j.msea.2009.04.046.

[19] P. Cavaliere, M. Cabibbo, F. Panella, A. Squillace, 2198 Al – Li plates joined by Friction Stir Welding : Mechanical and microstructural behavior, Mater. Des. 30 (2009) 3622–3631. https://doi.org/10.1016/j.matdes.2009.02.021.

[20] P. Cavaliere, A. De Santis, F. Panella, A. Squillace, Effect of anisotropy on fatigue properties of 2198 Al – Li plates joined by friction stir welding, Eng. Fail. Anal. 16 (2009) 1856–1865. https://doi.org/10.1016/j.engfailanal.2008.09.024.

[21] C. Gao, Z. Zhu, J. Han, H. Li, Materials Science & Engineering A Correlation of microstructure and mechanical properties in friction stir welded 2198-T8 Al – Li alloy, Mater. Sci. Eng. A. 639 (2015) 489–499. https://doi.org/10.1016/j.msea.2015.05.038.

[22] Y. Tao, D.R. Ni, B.L. Xiao, Z.Y. Ma, W. Wu, R.X. Zhang, Y.S. Zeng, Materials Science & Engineering A Origin of unusual fracture in stirred zone for friction stir welded 2198-T8 Al-Li alloy joints, 693 (2017) 1–13. https://doi.org/10.1016/j.msea.2017.03.079.

[23] B.T. Gibson, M.C. Ballun, G.E. Cook, A.M. Strauss, Friction stir lap joining of 2198 aluminum – lithium alloy with weaving and pulsing variants, J. Manuf. Process. 18 (2015) 12–22. https://doi.org/10.1016/j.jmapro.2014.12.002.

[24] M. Reimann, J. Goebel, T.M. Gartner, J.F. dos Santos, Refilling termination hole in AA 2198–T851 by refill friction stir spot welding, J. Mater. Process. Technol. 245 (2017) 157–166. https://doi.org/https://doi.org/10.1016/j.jmatprotec.2017.02.025.

[25] Y. Song, X. Yang, L. Cui, X. Hou, Z. Shen, Y. Xu, Defect features and mechanical properties of friction stir lap welded dissimilar AA2024 – AA7075 aluminum alloy sheets, J. Mater. 55 (2014) 9–18. https://doi.org/10.1016/j.matdes.2013.09.062.

[26] P. Venkateswaran, A.P. Reynolds, Factors affecting the properties of Friction Stir Welds between aluminum and magnesium alloys, Mater. Sci. Eng. A. 545 (2012) 26–37. https://doi.org/https://doi.org/10.1016/j.msea.2012.02.069.

[27] M.R. Jandaghi, C. Badini, M. Pavese, Dissimilar friction stir welding of AA2198 and AA7475 : Effect of solution treatment and aging on the microstructure and mechanical strength, J. Manuf. Process. 57 (2020) 712–724. https://doi.org/10.1016/j.jmapro.2020.07.037.

[28] A. Astarita, A. Squillace, A. Scala, A. Prisco, On the critical technological issues of friction stir welding T-joints of dissimilar aluminum alloys, J. Mater. Eng. Perform. 21 (2012). https://doi.org/10.1007/s11665-011-0073-3.

[29] C. Velotti, A. Astarita, A. Squillace, S. Ciliberto, M.G. Villano, M. Giuliani, U. Prisco, M. Montuori, G. Giorleo, F. Bellucci, On the critical technological issues of friction stir welding lap joints of dissimilar aluminum alloys, Surf. Interface Anal. 45 (2013). https://doi.org/10.1002/sia.5277.

[30] M. Perrella, V.P. Berardi, E. Armentani, Mode I Fracture Toughness Evaluation of Adhesively Bonded Joints via J-Integral and DIC, (2020). https://doi.org/10.1002/masy.201900116.

[31] L. Boccarusso, A. Astarita, P. Carlone, F. Scherillo, F. Rubino, A. Squillace, Dissimilar friction stir lap welding of AA 6082 - Mg AZ31: Force analysis and microstructure evolution, J. Manuf. Process. 44 (2019) 376–388. https://doi.org/10.1016/j.jmapro.2019.06.022.

[32] S. Zimmer, L. Langlois, J. Laye, Experimental investigation of the influence of the FSW plunge processing parameters on the maximum generated force and torque, (2010) 201–215. https://doi.org/10.1007/s00170-009-2188-3.

[33] A. Astarita, A. Squillace, L. Carrino, Experimental Study of the Forces Acting on the Tool in the Friction-Stir Welding of AA 2024 T3 Sheets, J. Mater. Eng. Perform. 23 (2014). https://doi.org/10.1007/s11665-014-1140-3.

[34] R.S. Mishra, Z.Y. Ma, Friction stir welding and processing, 50 (2005) 1–78. https://doi.org/10.1016/j.mser.2005.07.001.

[35] P. Carlone, G.S. Palazzo, Influence of Process Parameters on Microstructure and Mechanical Properties in AA2024-T3 Friction Stir Welding, Metallogr. Microstruct. Anal. 2 (2013) 213–222. https://doi.org/10.1007/s13632-013-0078-4.

[36] K.P. Mehta, P. Carlone, A. Astarita, F. Scherillo, F. Rubino, P. Vora, Conventional and cooling assisted friction stir welding of AA6061 and AZ31B alloys, Mater. Sci. Eng. A. 759 (2019) 252–261. https://doi.org/10.1016/j.msea.2019.04.120.

[37] P. Carlone, A. Astarita, F. Rubino, N. Pasquino, Microstructural Aspects in FSW and TIG Welding of Cast ZE41A Magnesium Alloy, Metall. Mater. Trans. B Process Metall. Mater. Process. Sci. 47 (2016). https://doi.org/10.1007/s11663-015-0536-2.

[38] B.S. Naik, D.L. Chen, X. Cao, P. Wanjara, Microstructure and Fatigue Properties of a Friction Stir Lap Welded Magnesium Alloy, (1991). https://doi.org/10.1007/s11661-013-1728-5.

[39] S.H. Chowdhury, D.L. Chen, S.D. Bhole, X. Cao, P. Wanjara, Materials Science & Engineering A Lap shear strength and fatigue behavior of friction stir spot welded dissimilar magnesium-to-aluminum joints with adhesive, Mater. Sci. Eng. A. 562 (2013) 53–60. https://doi.org/10.1016/j.msea.2012.11.039.

[40] S. Babu, G.D. Janaki Ram, P. V. Venkitakrishnan, G.M. Reddy, K.P. Rao, Microstructure and Mechanical Properties of Friction Stir Lap Welded Aluminum Alloy AA2014, J. Mater. Sci. Technol. 28 (2012) 414–426. https://doi.org/10.1016/S1005-0302(12)60077-2.

[41] A. Astarita, C. Bitondo, A. Squillace, E. Armentani, F. Bellucci, Stress corrosion cracking behaviour of conventional and innovative aluminium alloys for aeronautic applications, Surf. Interface Anal. 45 (2013). https://doi.org/10.1002/sia.5234.

[42] H. Cahn, PHYSICAL METALLURGY, Elsevier B. Ser. I (1996) 1996. https://doi.org/10.1016/B978-0-444-89875-3.50040-5.

[43] H.T. Zhou, Q.B. Li, Z.K. Zhao, Z.C. Liu, S.F. Wen, Q.D. Wang, Hot workability characteristics of magnesium alloy AZ80-A study using processing map, Mater. Sci. Eng. A. 527 (2010) 2022–2026. https://doi.org/10.1016/j.msea.2009.12.009.

[44] S. Il Kim, Y.C. Yoo, Dynamic recrystallization behavior of AISI 304 stainless steel, Mater. Sci. Eng. A. 311 (2001) 108–113. https://doi.org/10.1016/S0921-5093(01)00917-0.

[45] A. Dehghan-Manshadi, M.R. Barnett, P.D. Hodgson, Recrystallization in AISI 304 austenitic stainless steel during and after hot deformation, Mater. Sci. Eng. A. 485 (2008) 664–672. https://doi.org/10.1016/j.msea.2007.08.026.

[46] M. Ueki, S. Horie, T. Nakamura, Critical condition for transition from multiple to single peak dynamic recrystallization, Scr. Metall. 19 (1985) 547–549. https://doi.org/10.1016/0036-9748(85)90132-2.

[47] X. Zhang, F. Ma, W. Zhang, X. Li, Kinetics of dynamic recrystallization in AA2024 aluminum alloy, Mod. Appl. Sci. 8 (2014) 47–52. https://doi.org/10.5539/mas.v8n6p47.

[48] G.Z. Quan, Y.P. Mao, G.S. Li, W.Q. Lv, Y. Wang, J. Zhou, A characterization for the dynamic recrystallization kinetics of as-extruded 7075 aluminum alloy based on true stress-strain curves, Comput. Mater. Sci. 55 (2012) 65–72. https://doi.org/10.1016/j.commatsci.2011.11.031.

[49] D. Fersini, A. Pirondi, Fatigue behaviour of Al2024-T3 friction stir welded lap joints, Eng. Fract. Mech. 74 (2007) 468–480. https://doi.org/https://doi.org/10.1016/j.engfracmech.2006.07.010.

[50] P. Cavaliere, A. Squillace, F. Panella, Effect of welding parameters on mechanical and microstructural properties of AA6082 joints produced by friction stir welding, J. Mater. Process. Technol. 200 (2008) 364–372. https://doi.org/10.1016/j.jmatprotec.2007.09.050.

Figures

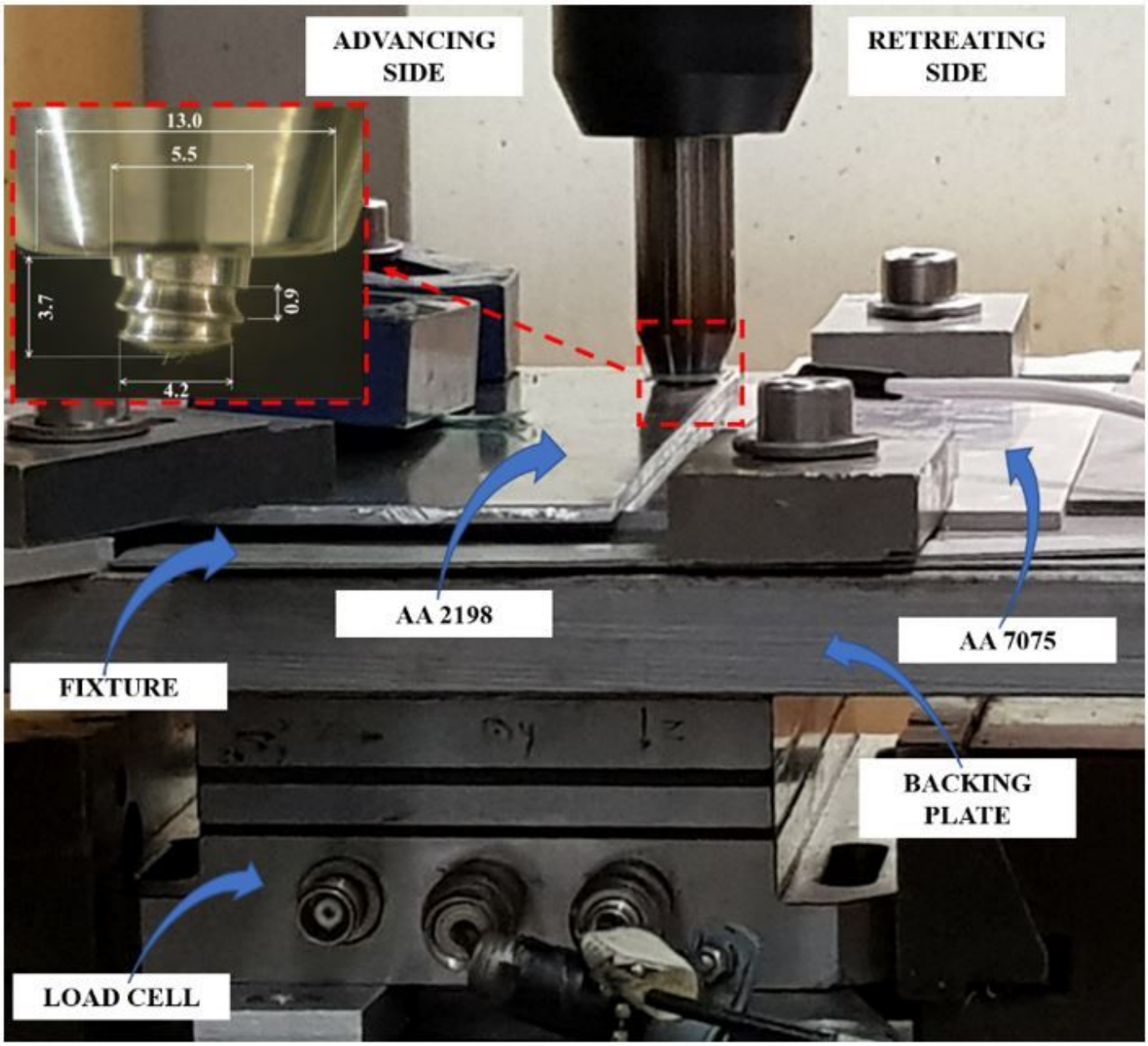

Figure 1

Adopted friction stir welding setup.

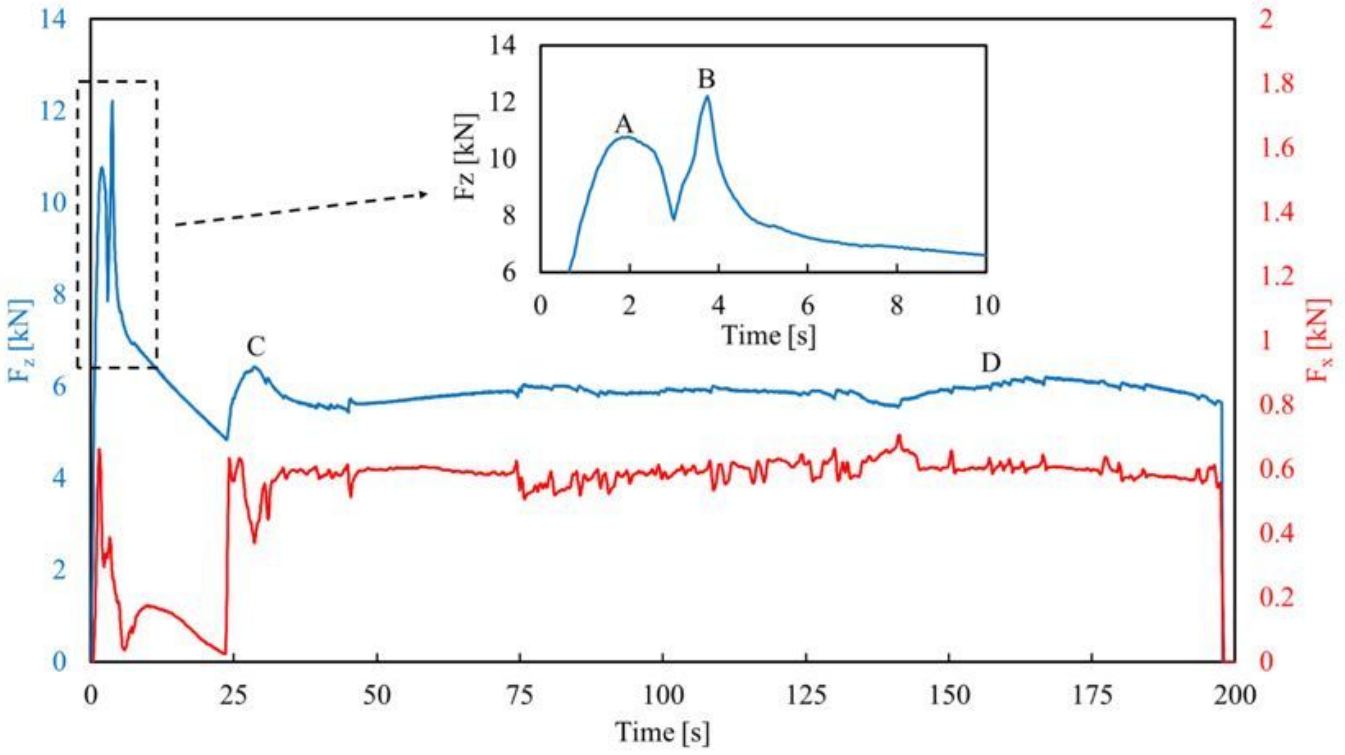

Figure 2

Representative force profiles, measured adopting TRS: 1200 rpm and WS: 60 mm/min.

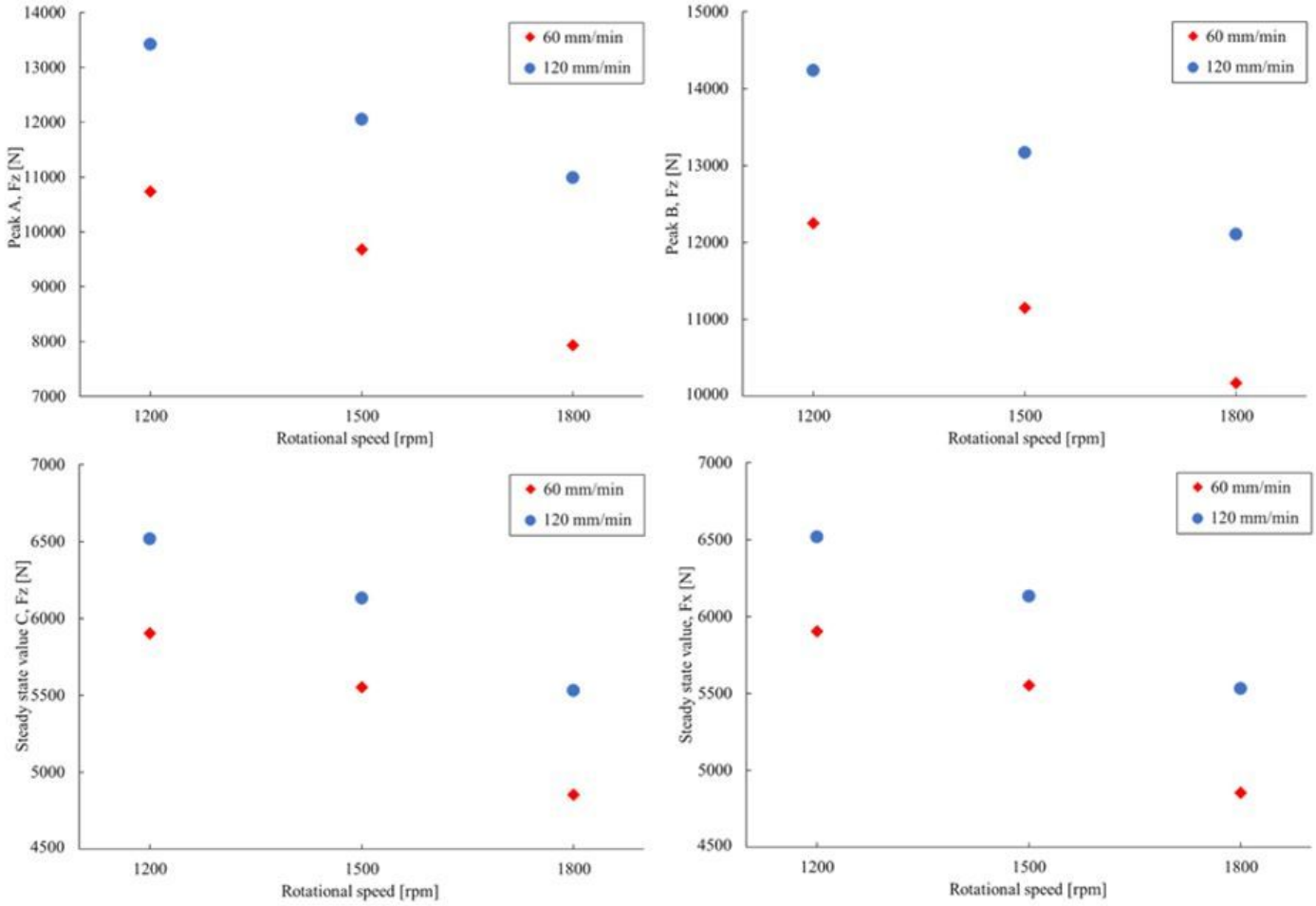

Figure 3

Peak and steady state values of the forces measured during the welding in all the processing conditions.

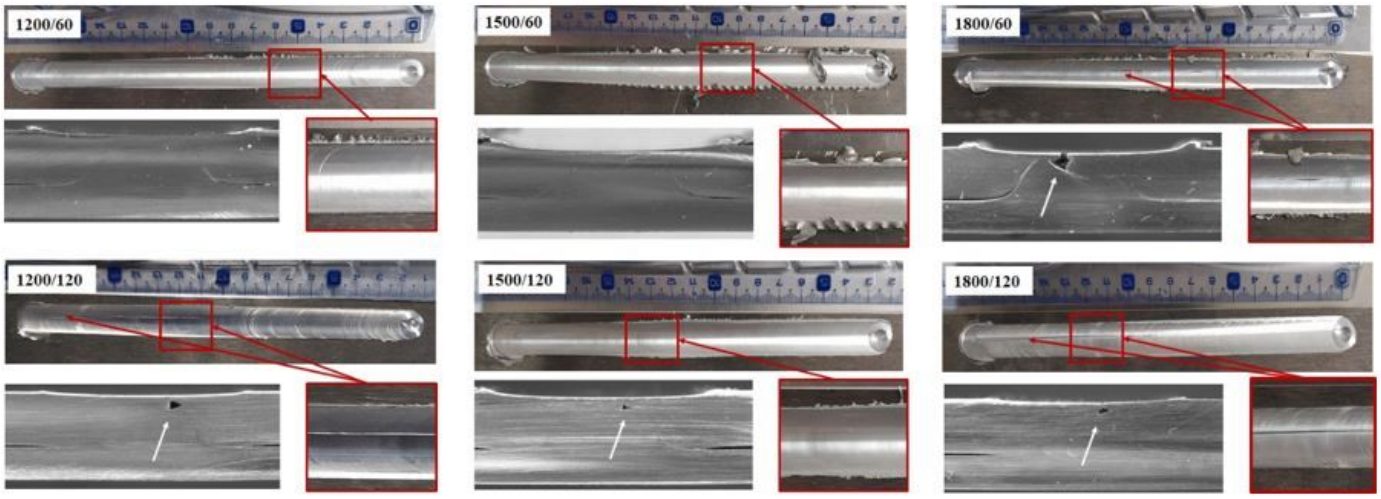

Figure 4

Cross sections and top surfaces of welded joints, including a close up of the crown (arrows highlight surface and internal defects as tunnel or groove).

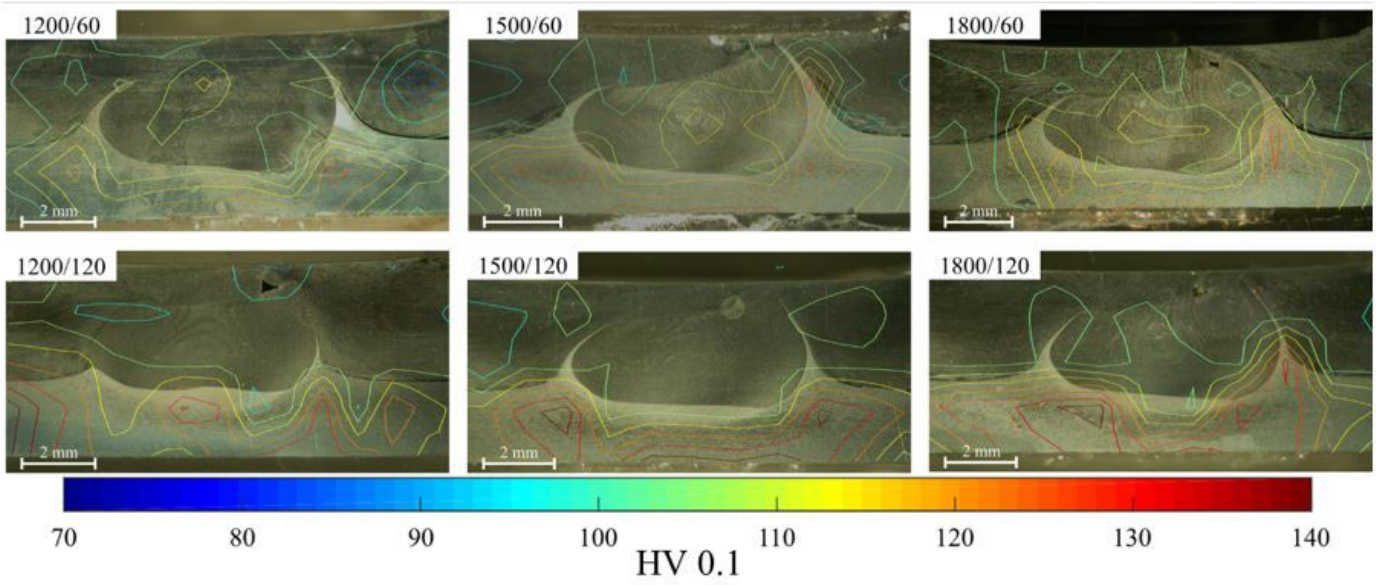

Figure 5

Optical observation of the polished and etched cross section, and representation of the microhardness distribution (advancing side on right hand side).

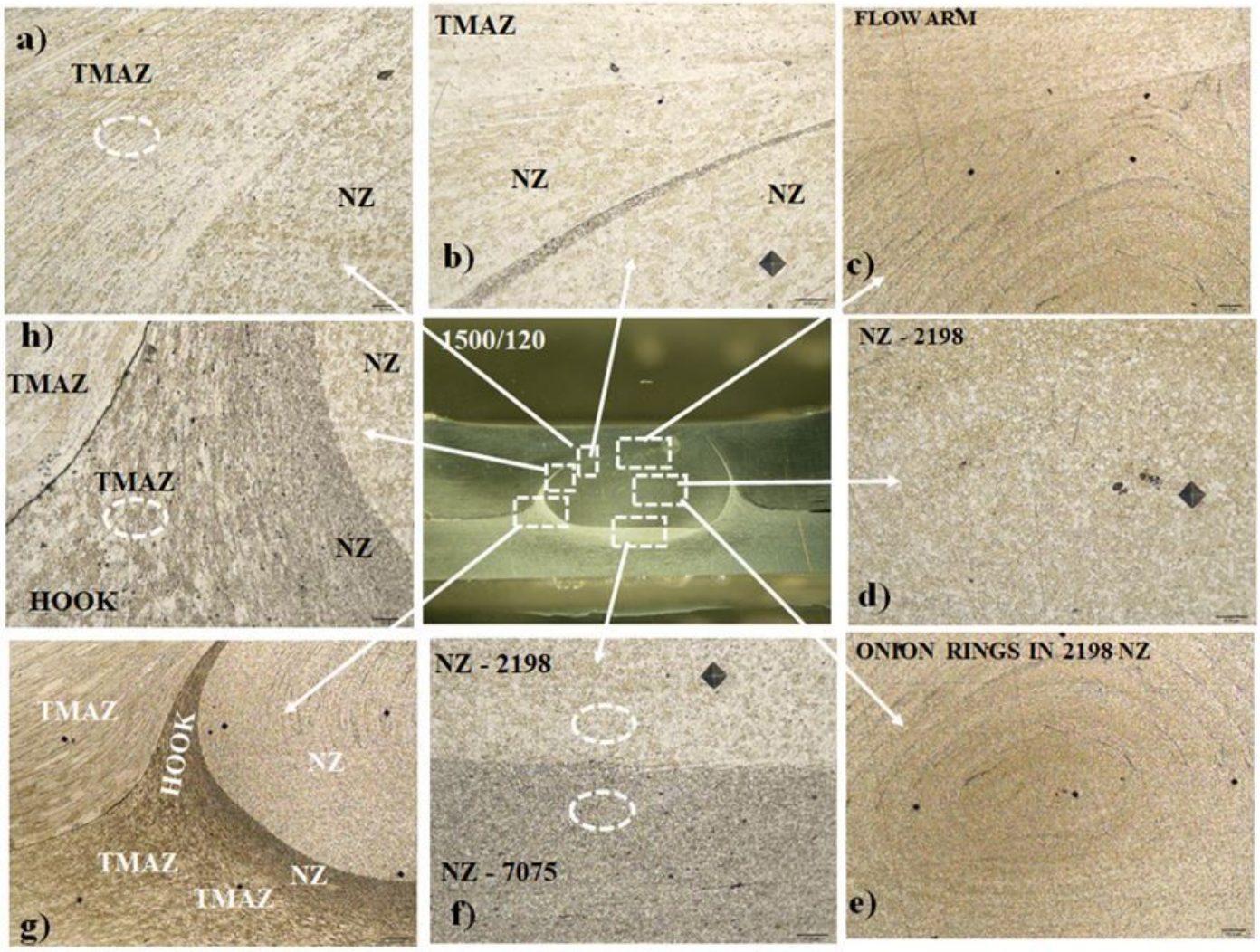

Figure 6

High magnification micrographs of the 1500/120 joint depicting the different metallurgical zones produced by the welding process.

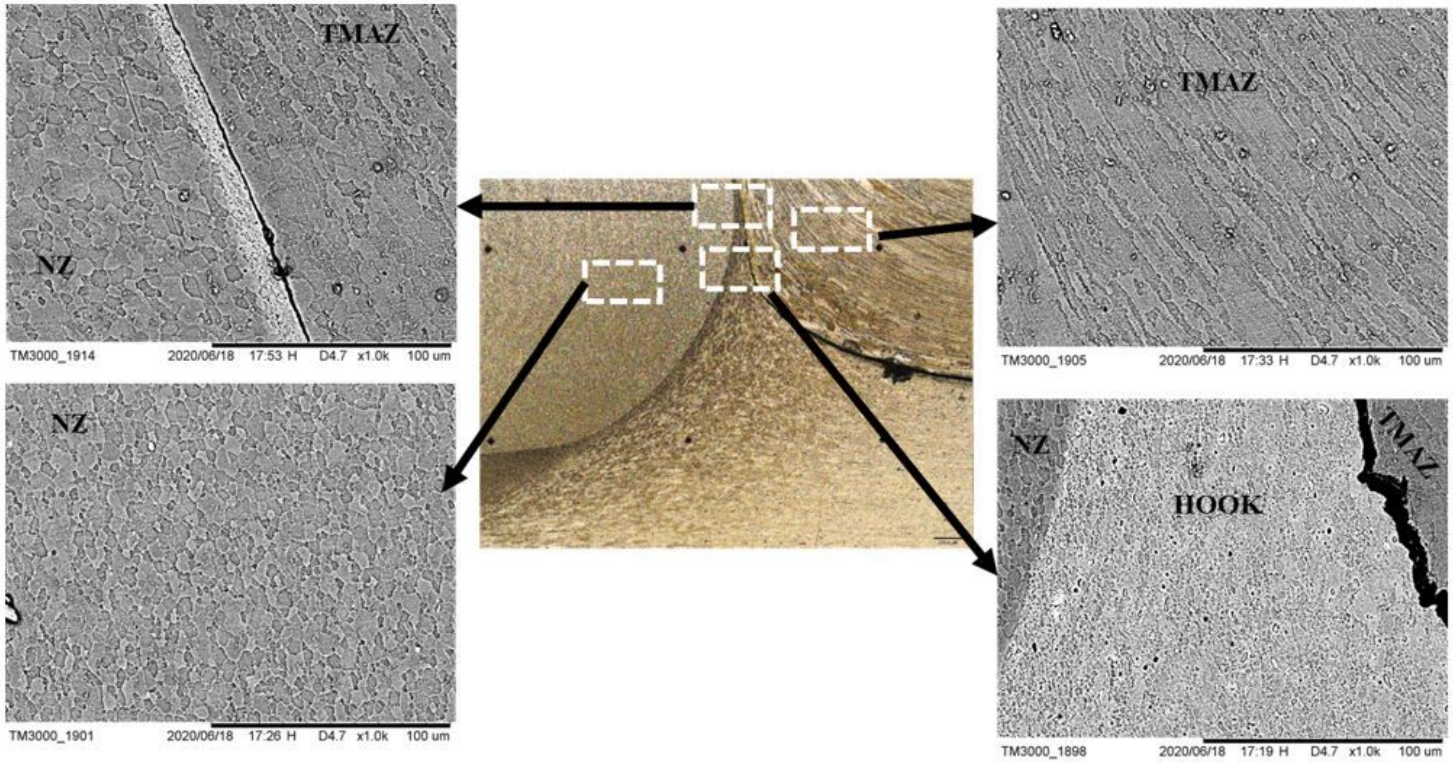

Figure 7

High magnification images of the hook in the advancing side of the joint.

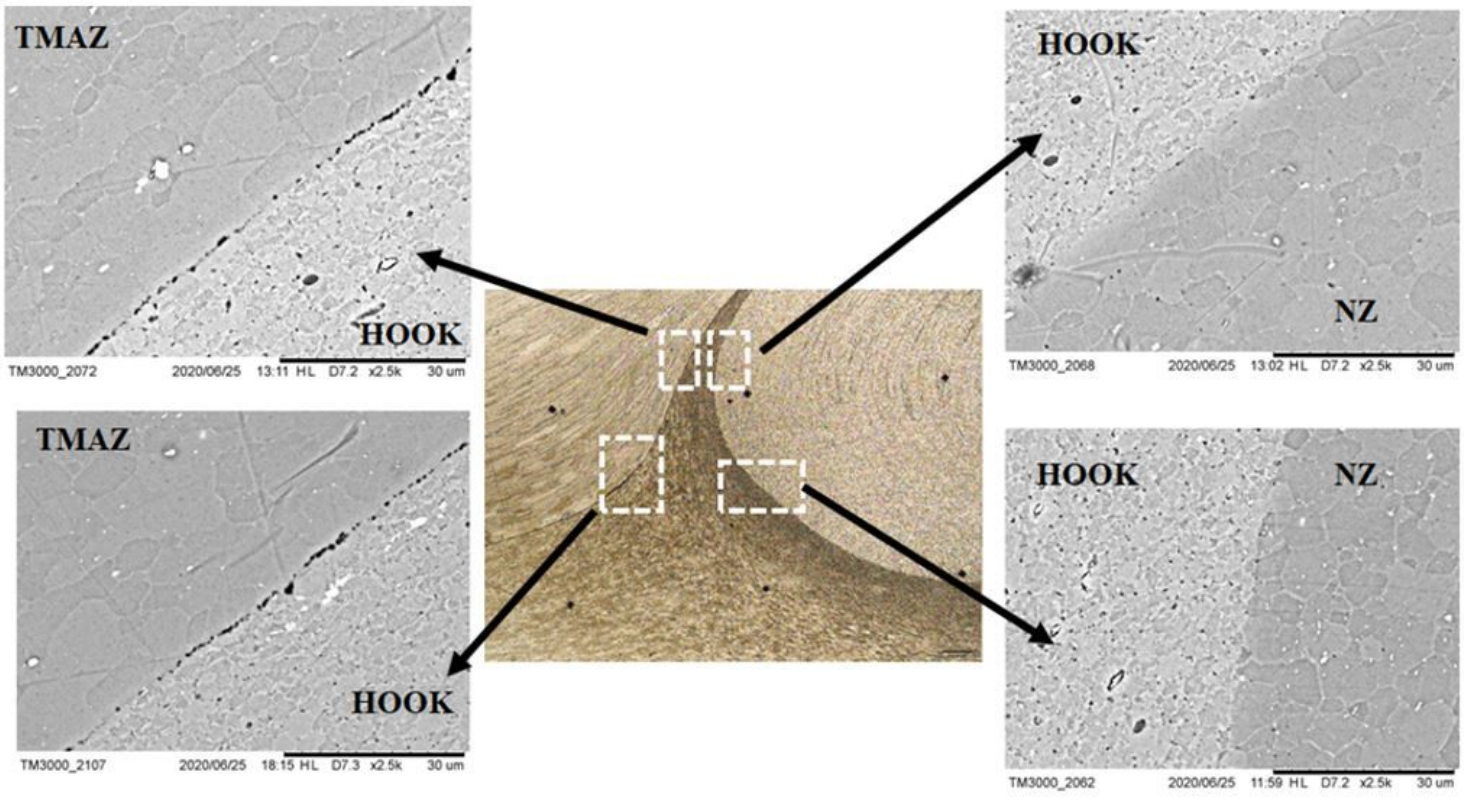

Figure 8

High magnification images of the hook in the retreating side of the joint.

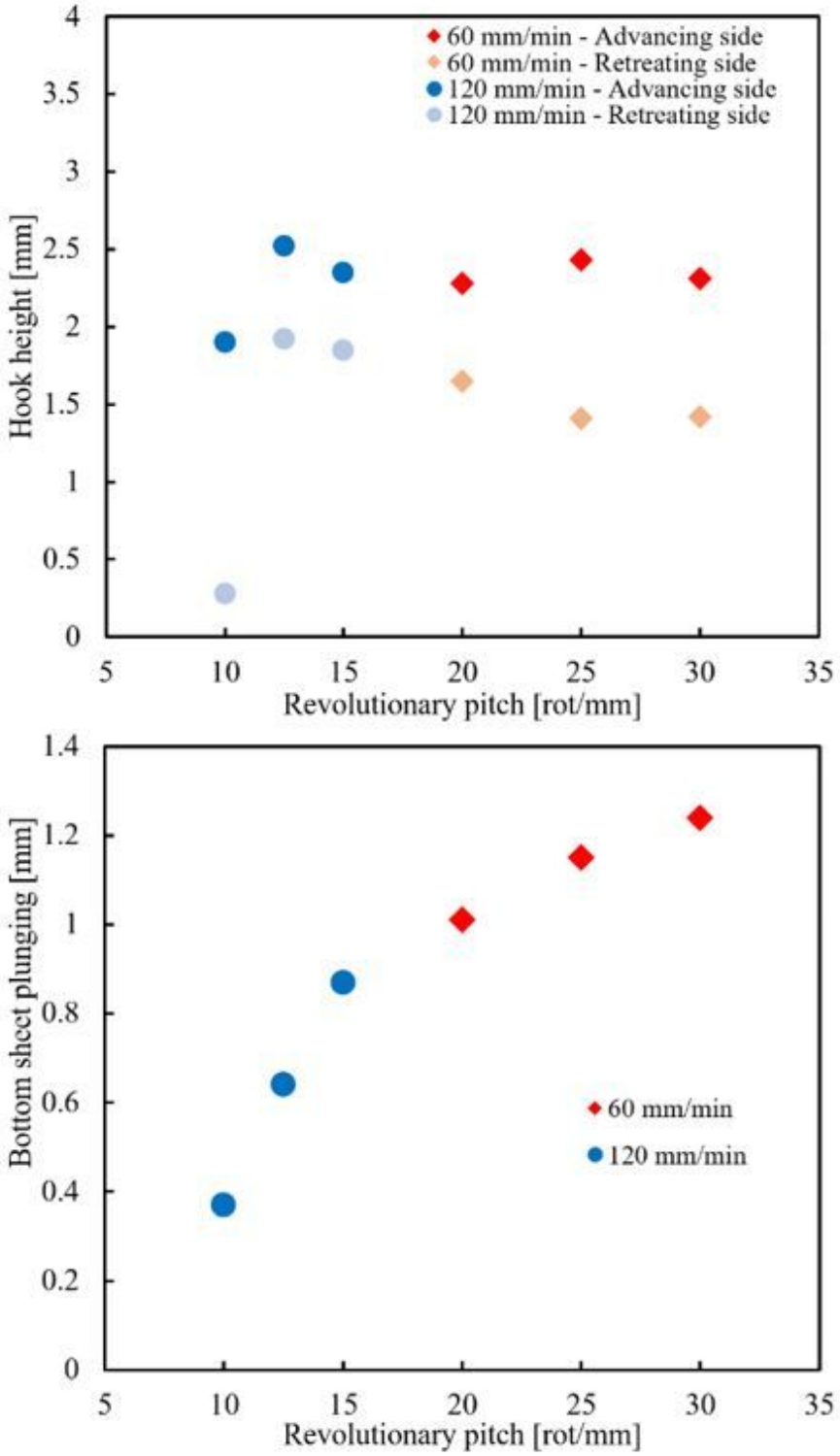

Figure 9

Geometrical details of the welding features (hook height on top and bottom sheet plunging on bottom) as a function of the revolutionary pitch.

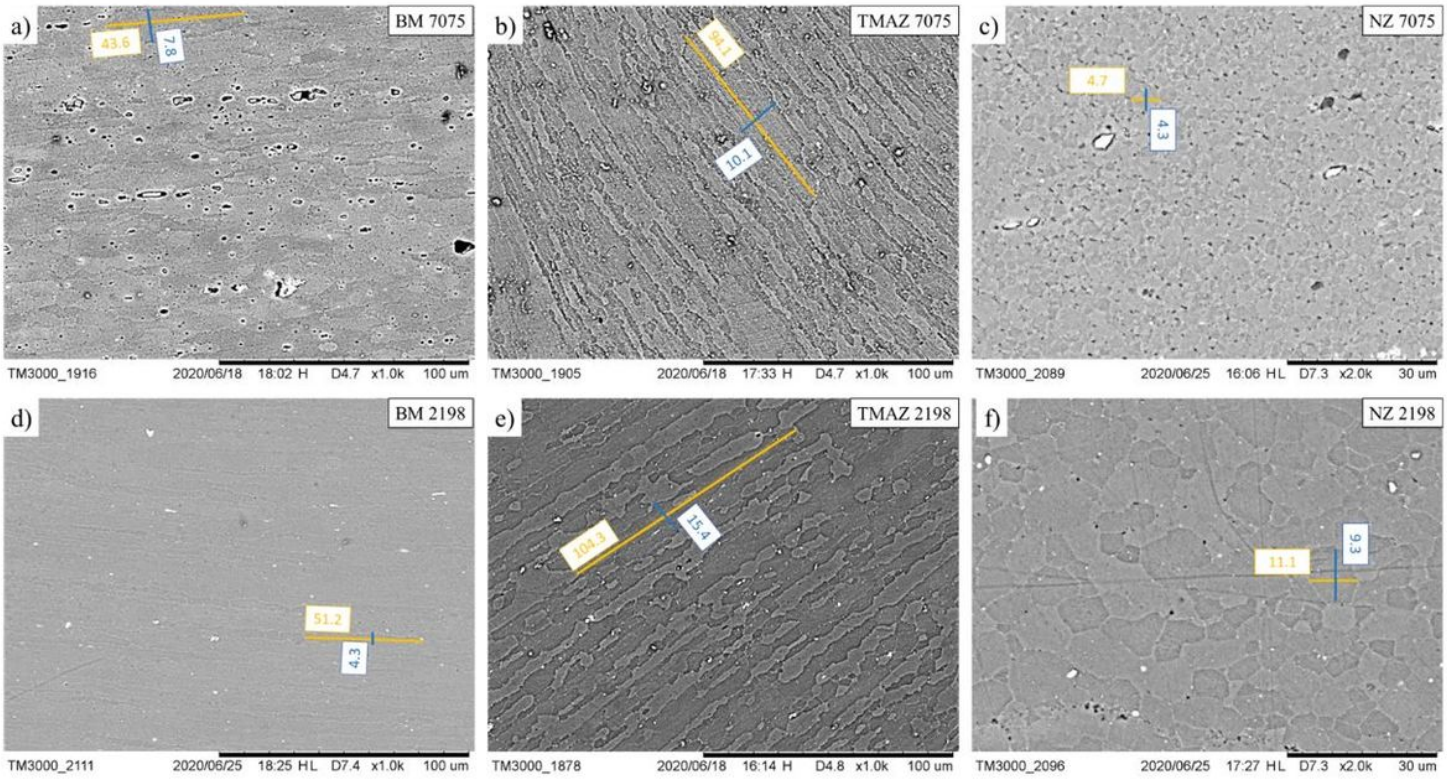

Figure 10

SEM micrographs of the grains structure of the AA 7075 at the BM (a), the TMAZ(b), and the NZ (c), and of AA 2198 at the BM (d), the TMAZ(e), and the NZ (f).

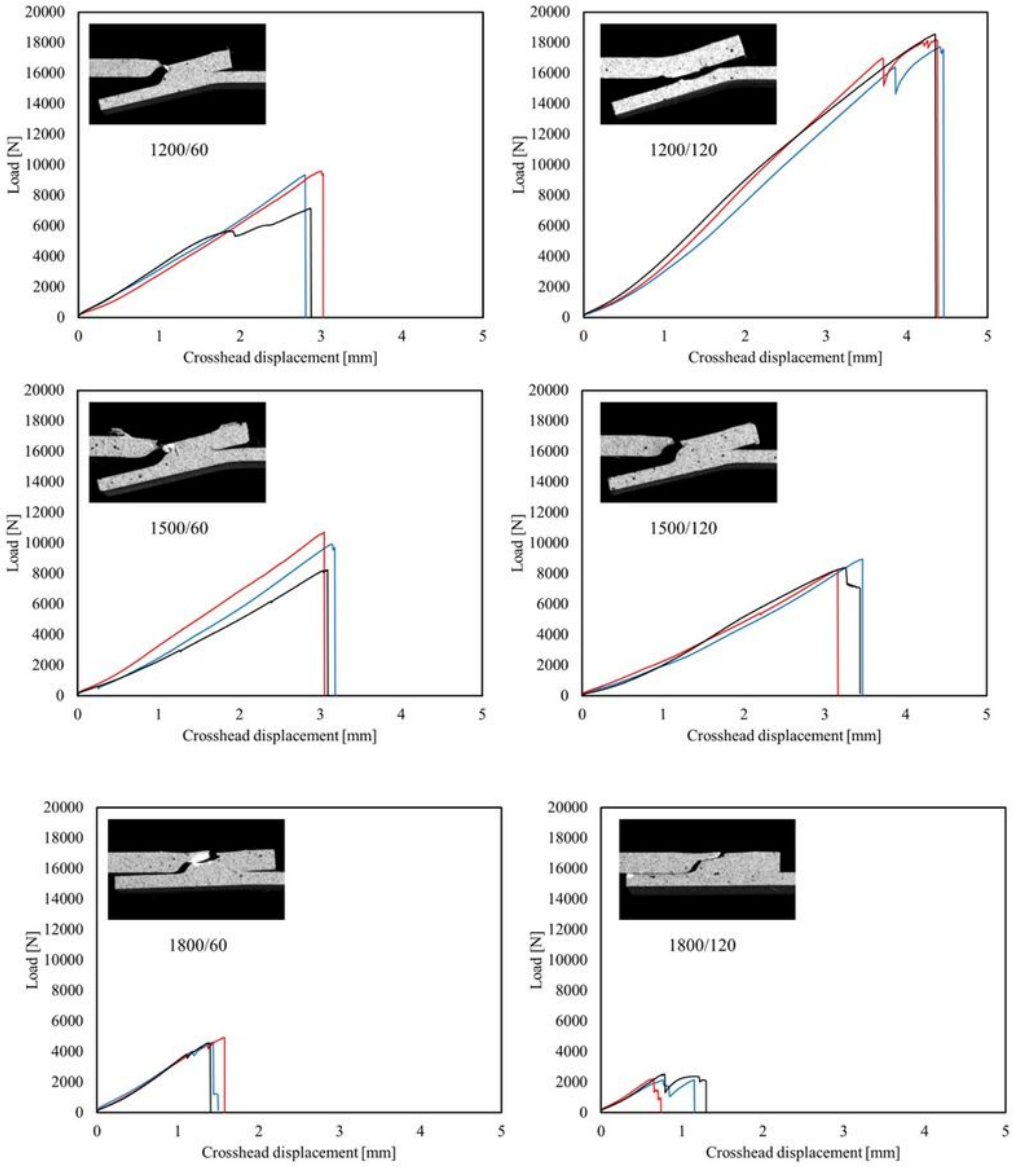

Figure 11

Lap shear behavior and failure of the welded joints.

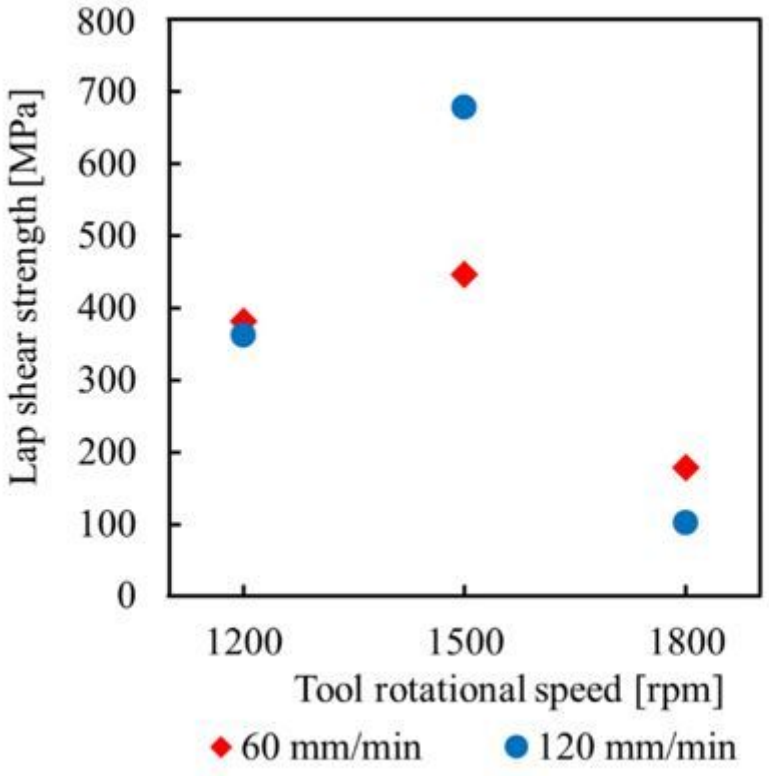

Figure 12

Lap shear strength variation with welding parameters.

Supplementary Files

This is a list of supplementary files associated with this preprint. Click to download.

- graphicalabstract.jpg